



# Physical properties and enhanced photocatalytic activity of ZnO-rGO nanocomposites

Poornima Sengunthar<sup>1</sup> · K. H. Bhavsar<sup>1</sup> · C. Balasubramanian<sup>2</sup> · U. S. Joshi<sup>1</sup>

Received: 20 March 2020 / Accepted: 22 June 2020 / Published online: 28 June 2020  
© Springer-Verlag GmbH Germany, part of Springer Nature 2020

## Abstract

Both zinc oxide (ZnO) and reduced graphene oxide (rGO) are known for its attractive optical properties in their nano form. Here, ZnO-rGO nanocomposites and rGO were prepared via simple and reproducible hydrothermal as well as modified Hummer's method. Microstructural identification of phase formation and dispersion of ZnO on rGO was confirmed by X-ray diffraction and transmission electron microscopy (TEM) measurements. The reduction of graphene oxide was confirmed by the appearance of D and G band peaks in Raman spectra. Optical bandgap of samples was estimated by UV-Visible diffused reflectance spectroscopy up to IR region. A systematic study of photocatalytic behavior towards the degradation of organic dyes such as methyl orange and rhodamine B under the influence of UV light source is demonstrated. Better than 85% of degradation was measured for both the dyes in the presence of ZnO-rGO composite during 2 h of UV illuminations. The enhanced photocatalytic activity of the composites is attributed to electron-hole charge transfer, which also promises its use in photovoltaics.

**Keywords** Reduced graphene Oxide(rGO) · ZnO-rGO nanocomposites · Photocatalytic activity

## 1 Introduction

Wastewater treatment has gained much attention due to widespread pollution and rapid global climate changes. A variety of methods has been employed to treat polluted water such as filtration, adsorption and incineration, and photocatalysis. Amongst all, photocatalytic activity has been proved to be efficient and environmentally friendly in removing pollutants from wastewater using light irradiation [1]. In the photocatalytic activity, under UV light irradiation,  $e^-$  are excited from the valence band to conduction band and form  $e^-$ -hole pair that are responsible for the degradation of pollutants using semiconducting material as a catalyst. The quick recombination of photogenerated  $e^-$ -hole pair results in quantum efficiency. A variety of electron-hole pair combination material have been widely studied such

as, semiconductor-nobel metal composite, carbon nanotube (CNTs), Graphene-semiconductor composite and so on [2].

A single layer of carbon known as Graphene( $sp^2$  bonded carbon atom arranged in hexagonal lattice) is a new material with a specific surface area of  $2620 \text{ m}^2/\text{g}$ , intrinsic strength of 130GPa and 0 eV bandgap has received much attention [3, 4]. On the other side, synthesis of graphene oxide(GO), and reduced graphene oxide(rGO) has stimulated interest because of different properties compared to graphite and graphene. Graphene oxide is a thin layer of carbon heavily decorated with hydroxyl and epoxy groups on  $sp^3$  carbon on the basal plane and carbonyl and a carboxyl group on  $sp^2$  bonded carbon atom whereas, rGO (two dimensional-2D) is obtained by reducing graphene oxide [5]. The C-O bonds disrupt the  $sp^2$  conjugation of carbon lattice resulting in the formation of GO- an insulator. On the other hand reducing the functional groups from GO increases the conductivity [6, 7]. Thus, GO and rGO plays a crucial role in controlling the structure and other properties [8]. A variety of methods have been reported for the synthesis of GO and its reduction. For the synthesis of GO, the most widely used methods are chemical vapor deposition, mechanical exfoliation, electron-beam evaporation, Hummer's method, and so on [9, 10]. The reduction of GO can be carried out via chemical,

✉ U. S. Joshi  
nexus2590@gmail.com; usjoshi@gmail.com

<sup>1</sup> Department of Physics, School of Sciences, Gujarat University, Ahmedabad 380009, India

<sup>2</sup> Atmospheric Plasma Division, F.C.I.P.T Campus, Institute for Plasma Research, Gandhinagar 382044, India

thermal, Optical and hydrothermal methods [11]. Thus, it is desirable to synthesize low cost, and facile rGO in large quantity [12]. Modified Hummer's method is one of the most accepted methods that has been used by researchers due to its high efficiency [8]. Whereas other reported methods for the production of GO and rGO require multiple steps for the synthesis as well as a variety of chemicals and solvents resulting in time-consuming approaches [13].

Meanwhile, many studies on combining rGO with suitable semiconductors have been attempted. Some of these combinations have shown promising photocatalytic and electronic applications because of charge transfer, magnetic and electronic interaction between the carbon atom and the semiconducting material [14–18]. Amongst other oxides, zinc oxide (ZnO) is highly preferred and widely studied due to its wide bandgap, high electron mobility which facilitates electron transfer and high exciton binding energy [19–22]. Many studies on the photocatalytic performance of ZnO-rGO nanocomposites have been reported. For example, X. Liu et al. reported on UV assisted synthesis of rGO-ZnO composites and maximum degradation of Cr(VI) under the UV light exposure [23]. X. Zhou et al. reported on hydrothermal synthesis of nanocomposites for degradation of methylene blue (MB) dye [24]. On the other hand, Y. Zhao et al. have synthesized three different shaped and morphologies of ZnO-rGO; namely, nanobowl (NB), nanorods (NR) and nanoparticles (NP) and the effect of shapes and morphology of ZnO-rGO nanocomposites of the photodegradation of RhB dye was reported [25]. The present report deals with a comparison of rGO and hydrothermally treated rGO with ZnO nanocomposites for photodegradation of industrially important dyes viz., methyl orange (MO) and rhodamine B (Rh B). The structural analysis of as-synthesized samples has been done using XRD and Raman spectroscopy. Optical properties were investigated to check the bandgap of the material. The photocatalytic activity of MO and RhB under the UV-light irradiation was studied using prepared samples as a catalyst. Furthermore, percentage degradation (% D) of dyes with increasing UV-light irradiation duration was also studied to check the wastewater treatment.

## 2 Experimental

### 2.1 Materials

Graphite powder with particle size 50  $\mu\text{m}$  (99.8%), sodium nitrate (AR grade),  $\text{H}_2\text{SO}_4$  (97%), potassium permanganate (AR grade), hydrogen peroxide (30%, ACS), hydrochloric acid (35%, ACS), hydrazine hydrate, zinc oxide (99.9%, AR), ethanol (AR) and deionized water was taken as starting materials for the synthesis of pure rGO and ZnO-rGO composites.

### 2.2 Synthesis of reduced graphene oxide (rGO)

The rGO is synthesized by modified Hummer's method which involves oxidation of graphite powder and reduction of oxidized graphite powder known as Graphene oxide [6]. Typically, graphite powder (2 g) with 50  $\mu\text{m}$  and sodium nitrate (2 g) was added to 90 ml concentrated  $\text{H}_2\text{SO}_4$  with constant stirring for 5 h in an ice bath. Under vigorous stirring,  $\text{KMnO}_4$  (12 g) was slowly added to the suspension to maintain the rate of the reaction below 20 °C. After 1 h stirring the mixture was diluted with distilled water (184 ml). The ice bath was then removed and the suspension was stirred for 2 h at 35 °C. Later, the mixture was treated with  $\text{H}_2\text{O}_2$  by which solution color changes from brown to yellow. Finally, the mixture was filtered and washed using centrifugation with 10% HCl and deionized water several times until pH becomes neutral. The resulting gel-like substance was dried in a hot air oven at 70 °C overnight. The collected solids known as graphene oxide were dissolved in hydrazine hydrate (strong reducing agent) with a ratio of 0.1:10 for 6 h at 100 °C. After the reduction process, the rGO was centrifuged with ethanol and deionized water to remove the impurities and dried overnight at 70 °C.

### 2.3 Hydrothermal synthesis of H.rGO and ZnO-rGO

Nanocomposites of rGO and ZnO-rGO were synthesized by one-step hydrothermal technique. Firstly, 30 mg of prepared rGO was dispersed in 30 ml of deionized water using sonication for 1 h and continued with stirring for 30 min. The prepared samples were transferred into 50 ml Teflon-lined stainless steel autoclave and heated at 180 °C for 24 h. The obtained precipitate (H.rGO) was washed with distilled water using centrifugation and dried at 70 °C for 6 h. Similarly, for the preparation of ZnO-rGO nanocomposites, 20 mg of rGO was dispersed in 20 ml of deionized water using sonication for 1 h. Then 0.15 M of ZnO solution was added dropwise to GO dispersion under continuous stirring for 2 h. The solution was transferred to autoclave and heated at 180 °C for 24–30 h. The final product (ZnO-rGO) was washed with deionized water and dried in a hot air oven for 6 h.

### 2.4 Photocatalytic experiment

Analytical grade Methyl Orange (MO) and Rhodamine B (Rh B) were used as the target organic dyes for the photocatalytic study. 10 mg of as-prepared samples, viz., ZnO, rGO, H.rGO, ZnO-rGO were added to 50 ml of dye solutions with  $1 \times 10^{-5}$  M concentration. The prepared solutions were ultrasonicated for 30 min followed by magnetic stirring for

1 h to establish the uniform dispersion and adsorption–desorption equilibrium. Then, solutions were exposed to UV light source having a wavelength of 254 nm and intensity of  $3.5 \text{ mW/cm}^2$  in a closed dark chamber. 5 mL of the reaction solutions were filled in the measuring cell for each measurement. The sample cell and reference cells were mounted in the UV–Vis–NIR Spectrophotometer (Shimadzu Corp, Model UV- 2600) and absorbance data were collected.

## 2.5 Characterization

Structural analysis of the prepared samples was done by using X-ray diffractometer (*Bruker, D8 Advance*) with copper sealed tube X-ray source producing Cu  $\alpha$  radiation at a wavelength of  $1.5406 \text{ \AA}$ . To check the shape, morphology and dispersion of material, transmission electron microscopy (TEM) was carried out (TEM, *FEI Technai G2 300 kV*). The synthesized powders are dispersed in iso-propyl alcohol and dropped on to carbon-coated copper grid used for TEM measurements. Raman spectra were recorded at room temperature by using Raman Spectroscopy consist of Argon ion laser with  $514.5 \text{ nm}$  wavelength (*Renishaw UK*). Optical properties were investigated by UV–Vis–NIR spectroscopy (*Shimadzu Corp, Model UV-2600*). The photocatalytic activity of two different dyes i.e., Rh B and MO were studied under UV light exposure and the corresponding absorbance of the degraded dyes was recorded using a liquid sample holder of the spectrophotometer.

## 3 Result and discussion

### 3.1 X-Ray diffraction (XRD) analysis

XRD patterns of rGO, H.rGO, and ZnO-rGO nanocomposites are shown in Fig. 1. Phase pure synthesis was observed and no impurity phases were identified. rGO and H.rGO exhibit almost similar pattern with little variation in their intensity and FWHM of (002) peak. Chemically reduced rGO exhibits pure hexagonal structure with an intense peak at  $26.55$  which corresponds to (002) diffraction plane. The broadening of (002) peak and formation of (101) and (004) peaks indicate larger interplanar spacing and decrease in intensity of peak is indicative of reduction of carbonyl and carboxyl group on the surface of the synthesized material. Hydrothermally treated rGO, reveals a further decrease in the intensity of peaks emphasizing more reduction on the surface as compared to chemically treated rGO [26, 27]. The formation of rGO-ZnO nanocomposites synthesized via hydrothermal technique exhibit pure phase of wurtzite structure with hexagonal symmetry with P63mc group [25]. The observed peaks correspond to the wurtzite ZnO structure are in agreement with the JCPDS card no 36–1451. The

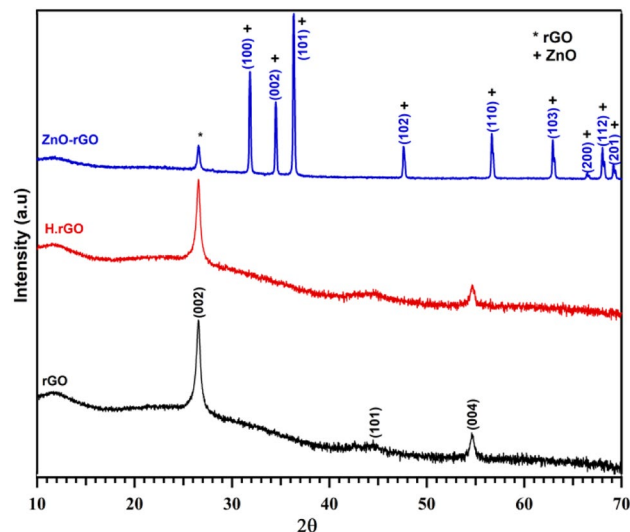


**Fig. 1** X-ray diffraction patterns of rGO, H.rGO, ZnO-rGO. All the peaks corresponding to differently synthesized rGO and ZnO-rGO-composites were indexed according to JCPDS files

**Table 1** Crystallite size of rGO, H.rGO, ZnO-rGO

Samples	XRD	Raman spectroscopy
	$t$ (nm)	$L_a$ (nm)
rGO	27.76	26.451
H.rGO	29.4	28.3
ZnO-rGO	35.88	38.44

broadening of ZnO peaks is found to be less which indicates the agglomeration of ZnO in rGO.

This is expected as the synthesis procedure of composites is done under high pressure [28]. The peak (002) at  $26.5$  confirms the presence of rGO in the nanocomposites. The occurrence of characteristics peaks of both rGO and ZnO confirms the formation of the nanocomposite. The crystallite sizes were calculated by using the Scherrer formula and are presented in Table 1.

### 3.2 TEM study

The dispersion and surface morphology of synthesized samples was studied by using TEM technique. Figure 2 shows TEM images of rGO (A&B) and ZnO-rGO (C&D) nanocomposites. Pure rGO revealed the successful formation of nanosheets with few layers and less folding. Darker areas reveal thick stacking of graphene layers with some oxygen functional groups. The higher transparency area indicates layer delamination due to the reduction mechanism [29]. Further, as observed in Fig. 2 (C&D), the rGO decorated on to the ZnO nanoparticle indicates strong binding interaction

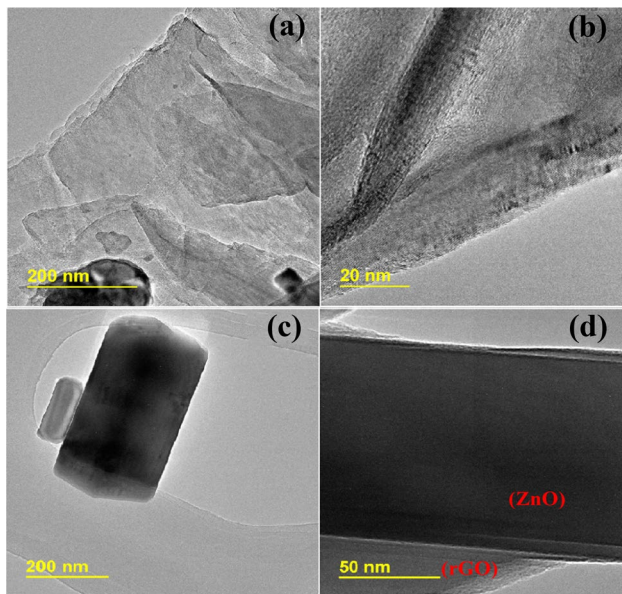


**Fig. 2** TEM images of pure rGO (A&B) and ZnO-rGO composites (C&D)

between rGO and ZnO resulting ZnO-rGO nanocomposite formation, which is also confirmed by XRD measurements. The average crystallite size was found less than 100 nm in each case [11].

### 3.3 Raman spectroscopy

rGO consists of partially healed carbon basal planes due to the removal of carboxyl, hydroxyl and carbonyl groups. Raman spectrum of carbon exhibits two prominent D-band and G-bands. In carbon atom, the D-band is associated with  $sp^3$  hybridization of edge defects on the carbon basal plane, and the G-band is associated with first-order scattering of the  $E_{2g}$  mode of the  $sp^2$  carbon atom in the hexagonal structure [30]. The Raman spectra of synthesized samples shown in Fig. 3 reveal the presence of both the bands with prominent G-band. Chemically reduced graphene oxide exhibits D-peak at  $1360\text{ cm}^{-1}$  which is due to disorder and defects in the hexagonal carbon framework and G-peak at  $1590\text{ cm}^{-1}$ , whereas H.rGO exhibits D-peak at  $1360\text{ cm}^{-1}$  and G-peak at  $1581\text{ cm}^{-1}$ , as shown in Fig. 3. The position of D-peak remains unchanged in both chemically reduced rGO and H.rGO, while G-peak shifts from  $1590\text{ cm}^{-1}$  to  $1581\text{ cm}^{-1}$  which may be due to self-healing characteristics of rGO that recover hexagonal framework of carbon atoms with defects [31]. In the case of ZnO-rGO nanocomposites, both disorder-defect and graphitic peak are found at  $1355\text{ cm}^{-1}$  and  $1581\text{ cm}^{-1}$ , respectively. The shift of D and G band in the nanocomposites sample is due to the addition of ZnO [32]. In addition, the intensity ratio of D to G-peaks is calculated

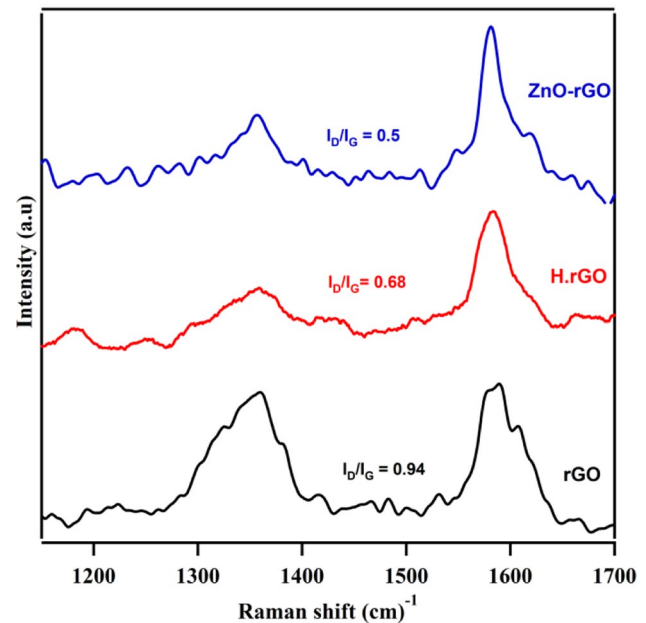


**Fig. 3** Raman Spectrum of rGO, H.rGO and ZnO-rGO

to measure the structural disorder. For chemically reduced rGO the ratio was found to be 0.94 which is decreased to 0.68 for H.rGO. Moreover, a slight decrease in the intensity ratio was observed to be 0.5 for the ZnO-rGO nanocomposites. The observed decrease in the value is may be due to the decrease in the  $sp^2$  domain size of carbon atoms and the reduction of  $sp^3$  to  $sp^2$  carbon during the hydrothermal process [31]. Using the intensity ratio from the Raman spectra, Fig. 3 the average crystallite size ( $L_a$ ) of  $sp^2$  domain is determined by modified Tuinstra -Koeing relation (Eq. 1) and is listed in Table 1 [33, 34].

$$L_a(\text{nm}) = (2.4 \times 10^{-10})\lambda^4 \times (I_D/I_G)^{-1} \quad (1)$$

It can be seen from Table 1, that the crystallite sizes estimated from XRD and Raman spectra are in good agreement with each other.

### 3.4 Optical properties

The optical behavior of synthesized powder samples was studied by UV-Vis.-NIR spectroscopy in the diffused reflectance mode. Figure 4(a) displays a typical reflectance spectrum of all synthesized samples from UV to IR range (220–1400 nm). From the result, chemically treated rGO and Hydrothermally treated rGO exhibits similar patterns with a small shift in the reflectance value for H.rGO, while the ZnO-rGO exhibits wide reflectance spectrum and decrease in reflectance above UV region ( $> 400\text{ nm}$ ) [35]. The peak around 250 nm for all samples is identified as  $\pi\text{-}\pi^*$  plasmon

peak which corresponds to aromatic C=C single bond and the presence of the peak in nanocomposites confirms the formation Zn–O–C bond [36]. Similarly, redshift in the spectra between rGO and H. rGO is due to the restoration of  $sp^2$  hybridization of the carbon atom and increase of electron concentration [37]. The visible light absorption is enhanced by the addition of rGO in the composite as zinc oxide strongly reflects visible light due to its white color.

Further, optical energy band gaps were calculated by applying Kubelka–Munk formula,

$$(\alpha h\nu)^{1/2} = C(h\nu - 2E_g) \quad (2)$$

where,  $\alpha$  is absorption coefficient,  $h$  is Planck's constant,  $\nu$  is frequency of light,  $\lambda$  wavelength,  $E_g$  is optical energy bandgap,  $C$  is proportionality constant and  $n = 1/2$  and  $2$  for direct and indirect bandgap materials, respectively [38]. Figure 4(b) shows Kubelka Munk plot where band gap energies are estimated from extrapolated lines. From Eq. (2), the estimated band gap values for ZnO, rGO, H.rGO and ZnO-rGO were 3.3 eV, 1.3 eV, 1.4 eV, and 3.25 eV, respectively. It may be noted that the optical band gaps of oxides including ZnO may be fine-tuned by using defects and/or chemical substitution [39, 40].

### 3.5 Photocatalytic activity

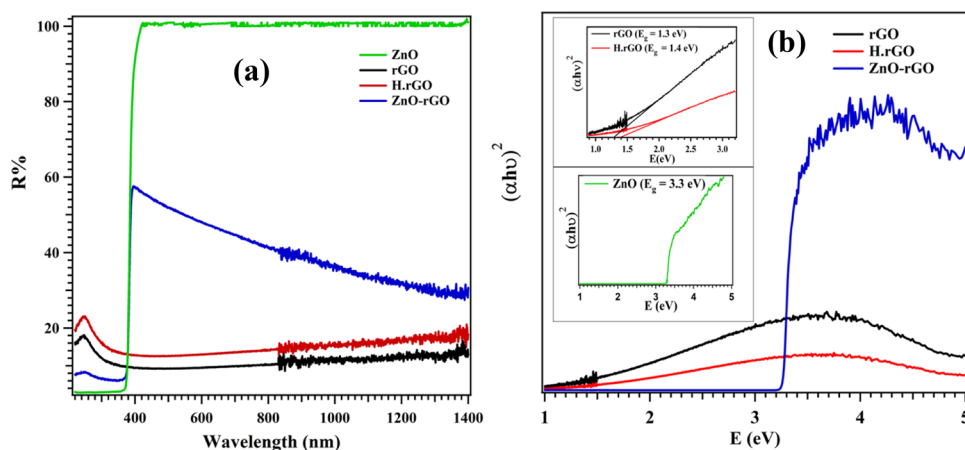
Photocatalysis is an extraordinary technique to degrade organic pollutants in water. Typically aqueous solution of organic pollutants containing semiconducting material as photocatalyst is irradiated under UV or Visible lights [41]. The reactive species involved in the photocatalytic degradation process are hole ( $h^+$ ), hydroxyl ( $\cdot OH$ ), and superoxide ( $O_2^-$ ) which are caused due to photo-induced reaction [28]. Further, the photocatalytic activity of bare ZnO is believed

to be due to the photoelectrons emitted by ZnO under the UV light exposure which in turn degrades the dye [24]. Here, the photocatalytic activity of as-prepared samples is evaluated by the degradation of two most commonly used industrial dyes, namely, methyl orange (MO) and Rhodamine B (Rh. B) under the UV light irradiation. The absorption spectra of dye with all synthesized samples are recorded at every 15 min and % D (percentage degradation) was calculated using the relation, [42]

$$\% D = \left(1 - \frac{A_t}{A_0}\right) \times 100 \quad (3)$$

where  $A_0$  is absorption before irradiation and  $A_t$  absorption at time  $t$  respectively. The results of the photocatalytic activities of MO by using ZnO, rGO, H.rGO, and ZnO-rGO are presented in Fig. 5. The figure shows actual photographs of degraded MO with rGO, H.rGO, and ZnO-rGO at different interval of illumination time with reference to the actual dye. Here, nominal 10% of the catalysts, viz, ZnO, rGO, H.rGO and ZnO-rGO were kept constant. As can be seen from Fig. 5, no significant changes are observed for ZnO sample while, the color of the dye drastically changes upon the addition of rGO, H.rGO and ZnO-rGO nanocomposites suggesting a rapid degradation of MO in presence of catalysts. Infact, the degradation of dye using ZnO-rGO nanocomposites is clearly higher than that of rGO and H.rGO. However, in the case of rGO and H.rGO, rGO was found better catalyst than H.rGO, as the reduction of oxygen functional group via chemical synthesis is significantly better than hydrothermally treated rGO [43]. The calculated percentage degradation of MO with 10% catalyst is shown in Table 2. An increase in illumination time results in a huge increase in the percentage of degradation. These results confirm that ZnO-rGO nanocomposites, even with 10 at. wt. %, have a significant effect in degrading the MO at room temperature.

**Fig. 4** **a** Diffused reflectance Spectra as a function of wavelength for pure ZnO, differently prepared rGO and ZnO-rGO composites, and **b** Tauc Plots. The inset shows extended range used for bandgap determination



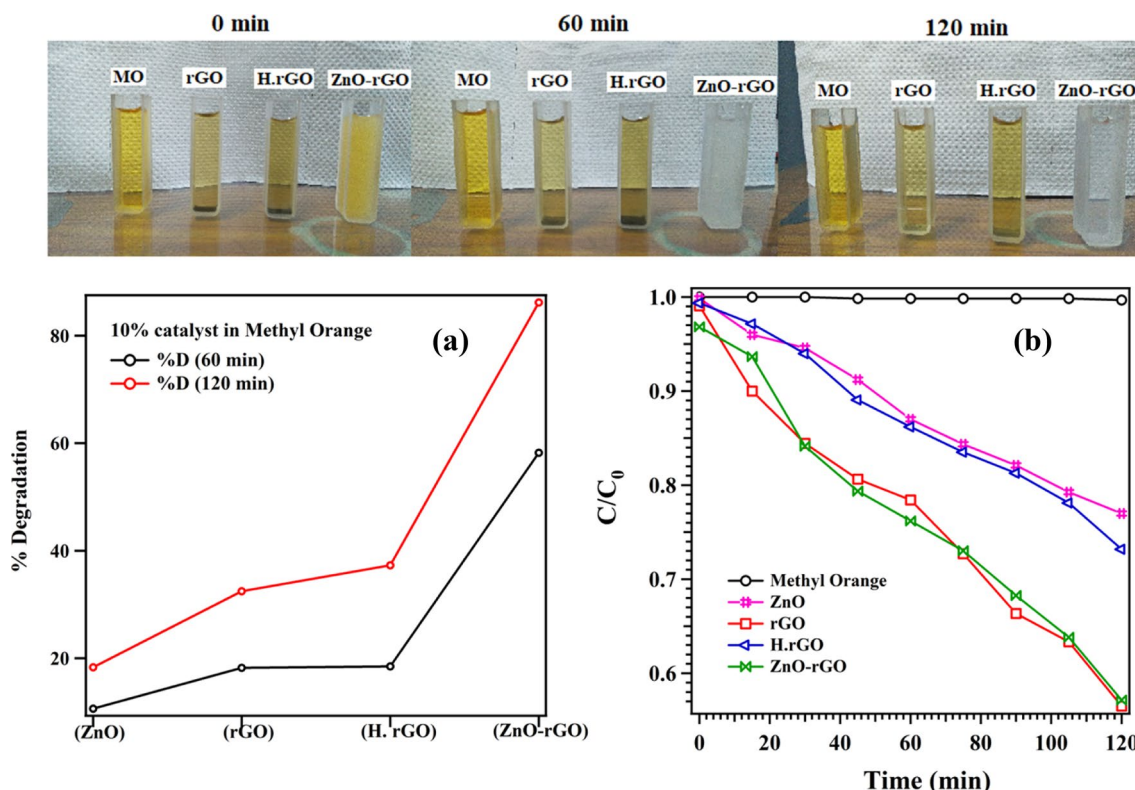


**Fig. 5** Actual photographs showing the degradation of MO with respect to illumination times for different catalysts under study. Completely colorless and transparent solutions suggest the complete deg-

radation efficiency of ZnO-rGO composites. Graphical representation of photocatalytic data is shown in (a) %Degradation versus catalyst and (b) concentration ratio ( $C/C_0$ ) versus time

The relation between ( $C/C_0$ ) and time for MO is plotted in Fig. 5 (b). In the absence of catalyst, the change in the concentration is linear with respect to time because of minor degradation under the UV light irradiation. Here again, a very sharp and monotonous decrease in the degradation rate constant is clearly visible in Fig. 5(b), for ZnO-rGO nanocomposites as compared to rGO and/or H.rGO.

Similarly, the photocatalytic activity of Rhodamine B. (Rh.B) using rGO, H.rGO, ZnO-rGO as a catalyst is shown in Fig. 6. The Photograph displays degraded Rh.B with and without catalyst with increasing illumination time. Here, a nominal 10% catalyst was kept constant. As shown in photograph and Fig. 6(a) the color of Rh.B dye

drastically changes upon the addition of catalyst suggesting a rapid degradation of dye, infact the dye gets completely degraded using ZnO-rGO nanocomposites like in case of MO. In the case of rGO and H.rGO degradation is not as significant as compared to ZnO-rGO. The calculated % degradation is listed in Table 2.

The values directly indicate an increase in % degradation with increasing illumination time. Thus result confirms that nanocomposites with 10% have a huge effect in degrading the Rh.B at room temperature [44]. The higher degradation in ZnO-rGO is due to the presence of rGO, which transfer  $e^-$  quickly [45]. Reports also suggest that the presence of rGO provides an excess surface area which binds the dye molecules through  $\pi$ - $\pi$  conjugation with the offset [46]. The relation between ( $C/C_0$ ) and time are plotted for Rh.B shown in Fig. 6(b). In the absence of catalyst, the change in concentration is linear with respect to time. Figure 6 (b) reveals, constant decrease in the concentration of dye with illumination time. Apparently, the presence of rGO in the composite enhances the photocatalytic property with increasing illumination time.

**Table 2** % degradation of dye w.r.t. illumination time

Catalyst	%D of Methyl Orange		%D of Rhodamine B	
	60 min	120 min	60 min	120 min
rGO	18.21	32.45	41.41	49.56
H.rGO	18.48	37.28	43.28	52.17
ZnO-rGO	58.22	86.16	69.21	87.21

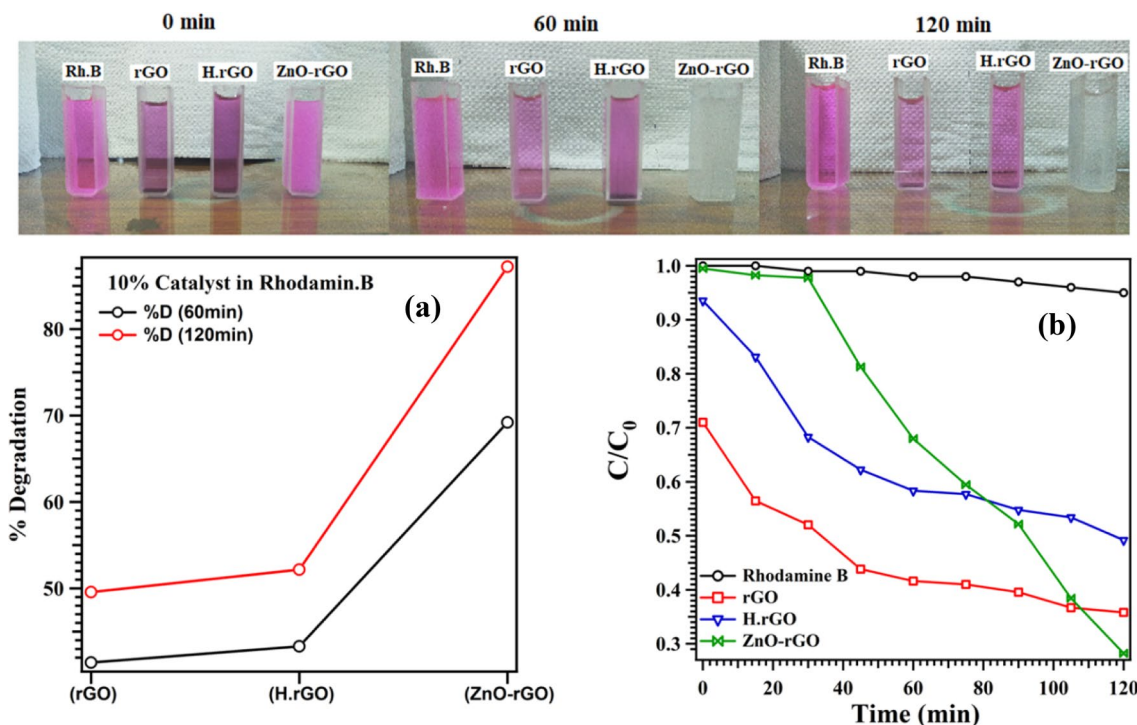
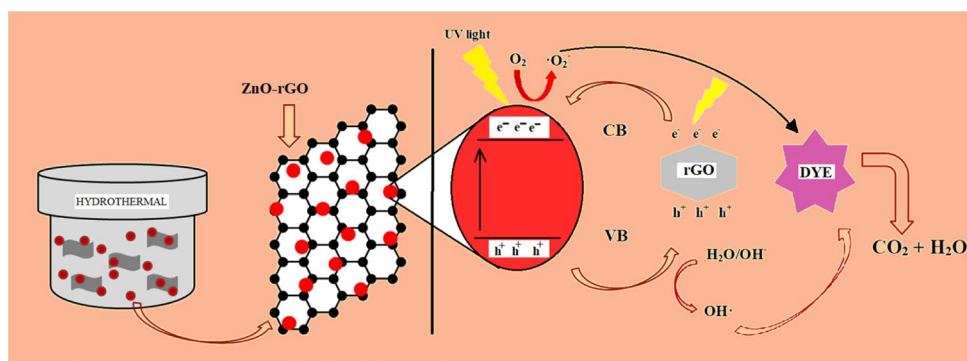


**Fig. 6** Photographs showing the degradation of Rh B with respect to illumination times for rGO, H.rGO, and ZnO-rGO composites. Completely colorless and transparent solutions suggest the complete deg-

radation efficiency of ZnO-rGO composites. Graphical representation of photocatalytic data is shown in (a) % Degradation versus catalyst and (b) concentration ratio ( $C/C_0$ ) versus time

**Fig. 7** Schematic of photocatalytic activity using ZnO-rGO nanocomposites



### 3.6 Mechanism of photocatalysis of ZnO-rGO as a catalyst

Semiconducting material with wide bandgap serves as a good catalyst in the photocatalysis process. When photons from light sources are bombarded on the aqueous organic pollutants containing semiconducting material, it produces pairs of electron and holes. In the proposed mechanism, as shown in Fig. 7, ZnO nanoparticles in the composite absorb UV photons and produce electron-hole pairs. Then, this excited electron reacts with surface oxygen of solution to

form superoxide radicals ( $O_2^-$ ) and photogenerated holes combine with the oxygen and form ( $\cdot OH^-$ ). rGO accepts this radical as it has a fermi level below the conduction band of ZnO. This offers a path for the excited electron of the valance band of ZnO to jump into the valence band of rGO [9, 25, 45, 47]. rGO works as co-catalyst for the rapid transfer of photogenerated carriers, which is due to excellent conductivity and this results in subsequent charge separation [48, 49]. Finally, the radicals react with the organic pollutants and form  $CO_2$ ,  $H_2O$  and other by-products as depicted in Fig. 7.

## 4 Conclusions

In the present work, chemically reduced graphene oxide (rGO), hydrothermally derived rGO and ZnO-rGO nanocomposites are synthesized by a modified chemical process and characterized by structural, Raman, and optical properties. Phase pure hexagonal structure of rGO and wurtzite structure of ZnO-rGO is confirmed by XRD. The Raman spectra show the presence of clear D and G bands with a decrease in the D to G band ratio for ZnO-rGO nanocomposites; which is attributed to the decrease in the  $sp^2$  domain size of carbon atoms and the reduction of  $sp^3$  to  $sp^2$  carbon during the growth process. TEM analysis revealed the successful formation of rGO nanosheets with few layers without any folding. Strong binding of ZnO-rGO nanocomposite was also revealed by TEM. Optical spectroscopy results show an enhancement in the visible range and are attributed to an increase of surface electron charge of oxides in the composite and alteration in the process of electron–hole pair formation during light illumination. Our results are suggestive of the potential of ZnO-rGO nanocomposites in the utilization of solar energy applications. Photocatalytic activity of rGO, H.rGO and ZnO-rGO nanocomposites were examined for two commonly used industrial dyes, the MO and Rhodamine B. Nearly complete degradation of these dyes was achieved by using ZnO-rGO nanocomposites at room temperature.

**Acknowledgement** USJ thank DST and UGC, India for FIST and SAP (I) projects, respectively.

## References

- N. Kumaresan, M. M. A. Sinthiya, K. Ramamurthi, R. Ramesh Babu, and K. Sethuraman, *Arab. J. Chem.* (2019).
- Q. P. Luo, X. Y. Yu, B. X. Lei, H. Y. Chen, D. Bin Kuang, and C. Y. Su, *J. Phys. Chem. C* **116**, 8111 (2012).
- G. Eda, G. Fanchini, M. Chhowalla, *Nature Nanotech.* **3**, 1–5 (2008).
- K. S. Novoselov, A. K. Geim, S. V. Morozov, D. Jiang, A. A. Firsov, Y. Zhang, S. V. Dubonos, I. V. Grigorieva, M. Chuang, S. Nielsen, J. M. Haroche, M. Raimond, F. Brune, De, C. Martini, E. M. D. Monroe, and Barrett, *Science*, **306**, 666–669 (2004).
- D. Hou, Q. Liu, X. Wang, Y. Quan, Z. Qiao, and L. Yu, *J. Mater. Chem.* **4**, 256–265 (2018).
- B. Paulchamy, G. Arthi, L. Bd, *J. Nanomed. Nanotechnol.* **6**, 1–4 (2015).
- D. Konios, M.M. Stylianakis, E. Stratakis, E. Kymakis, *J. Colloid Interface Sci.* **430**, 108–112 (2014).
- J. Chen, B. Yao, C. Li, G. Shi, *Carbon* **64**, 225–229 (2013).
- S. Meti, M.R. Rahman, I. Ahmad, K.U. Bhat, *Appl. Surf. Sci.* **451**, 67–75 (2018).
- Y. Zhu, S. Murali, W. Cai, X. Li, J.W. Suk, J.R. Potts, R.S. Ruoff, *Adv. Mater.* **22**, 3906 (2010).
- F. Wu, Y. Xia, Y. Wang, and M. Wang, *J. Mater. Chem. A*, **2**, 20307 (2014).
- K. Ai, Y. Liu, L. Lu, X. Cheng, L. Huo, *J. Mater. Chem.* **21**, 3365 (2011).
- B. Sidhureddy, A. R. Thirupathi, and A. Chen, *Chem. Commun.* 7828 (2017).
- M. Azarang, A. Shuhaimi, R. Yousefi, S.P. Jahromi, *RSC Adv.* **5**, 21888 (2015).
- S. Bai, X. Shen, *RSC Adv.* **2**, 64 (2012).
- J. Tian, S. Liu, H. Li, L. Wang, Y. Zhang, Y. Luo, A.M. Asiri, A.O. Al-Youbi, X. Sun, *RSC Adv.* **2**, 1318 (2012).
- M. Sookhaskian, Y.M. Amin, R. Zakaria, W.J. Basirun, M.R. Mahmoudian, B. Nasiri-Tabrizi, S. Baradaran, M. Azarang, *J. Alloys Compd.* **632**, 201 (2015).
- W. Long, L. Fu, *Fullerenes Nanotub. Carbon Nanostructures* **25**, 404 (2017).
- A. Pruna, J. Cembrero, D. Pullini, A. M. Mocioiu, and D. Busquets-Mataix, *Appl. Phys. A Mater. Sci. Process.* **123**, 0 (2017).
- B.V. Mistry, U.S. Joshi, *Aip. Conf. Proc.* **080002**, 1 (2018).
- F.C. Romeiro, M.A. Rodrigues, L.A.J. Silva, A.C. Catto, F. Luis, E. Longo, E. Nossol, R.C. Lima, *Appl. Surf. Sci.* **423**, 743 (2017).
- S. Yang, G. Li, L. Qu, G. Wang, and D. Wang, *RSC Adv.* **7**, 35004 (2017).
- X. Liu, L. Pan, Q. Zhao, T. Lv, G. Zhu, T. Chen, T. Lu, Z. Sun, C. Sun, *Chem. Eng. J.* **183**, 238 (2012).
- X. Zhou, T. Shi, H. Zhou, *Appl. Surf. Sci.* **258**, 6204 (2012).
- Y. Zhao, L. Liu, T. Cui, G. Tong, W. Wu, *Appl. Surf. Sci.* **412**, 58 (2017).
- C. Montaser, M. Blanco, E. Aranzabe, and A. Aranzabe, *Polymer*, **9** (2017).
- S. N. Alam, N. Sharma, and L. Kumar, *Graphene*, **6**, 1–18 (2017).
- S. Kumar, K. Dutta, S. Pal, S. Mandal, A. Naskar, D. Jana, *Mater. Chem. Phys.* **223**, 456 (2019).
- L. Stobinski, B. Lesiak, A. Malolepszy, M. Mazurkiewicz, B. Mierzwa, J. Zemek, P. Jiricek, I. Bieloshapka, *J. Electron Spectros. Relat. Phenomena* **195**, 145 (2014).
- A. C. Ferrari and J. Robertson, *Phys. Rev. B - Condens. Matter Phys.* **64**, (2001).
- G.T. Soon How, A. Pandikumar, H. N. Ming, and L. H. Ngee, *Sci. Rep.* **2**, (2014).
- J. Ding, S. Zhu, T. Zhu, W. Sun, Q. Li, G. Wei, Z. Su, *RSC Adv.* **5**, 22935 (2015).
- T.N. Lin, K.H. Chih, C.T. Yuan, J.L. Shen, C.A.J. Lin, W.R. Liu, *Nanoscale* **7**, 2708 (2015).
- L.G. Capado, K. Takai, T. Enoki, M. Endo, Y.A. Kim, H. Mizusaki, A. Jorio, L.N. Coelho, R. Magalhães-Paniago, M.A. Pimenta, *Appl. Phys. Lett.* **88**, 163106 (2006).
- H. N. Tien, V. H. Luan, L. T. Hoa, N. T. Khoa, S. H. Hahn, J. S. Chung, E. W. Shin, and S. H. Hur, *Chem. Eng. J.* (2013).
- E. Kusiak-Nejman, D. Moszyński, J. Kapica-Kozar, A. Wanag, A. Morawski, *Nanomaterials* **8**, 647 (2018).
- C.P.P. Wong, C.W. Lai, K.M. Lee, S. Bee, A. Hamid, *Materials* **8**, 7118 (2015).
- Y. Feng, N. Feng, Y. Wei, G. Zhang, *RSC Adv.* **4**, 7933 (2014).
- B. V. Mistry, D. K. Avasthi, and U. S. Joshi, *Appl. Phys. A Mater. Sci. Process.* **122**, (2016).
- S.J. Trivedi, S.A. Khan, U.S. Joshi, *Radiat. Eff. Defects Solids* **168**, 532 (2013).
- A. Fujishima, K. Honda, *Nature* **238**, 37 (1972).
- R. Chauhan, A. Kumar, and R. Pal Chaudhary, *J. Lumin.* **145**, 6 (2014).



43. I.O. Faniyi, O. Fasakin, B. Olofinjana, A.S. Adekunle, T.V. Oluwasusi, M.A. Eleruja, E.O.B. Ajayi, S.N. Appl. Sci. **1**, 1181 (2019)
44. X. Chen, Y. He, Q. Zhang, L. Li, D. Hu, T. Yin, J. Mater. Sci. **45**, 953 (2010)
45. Y. Zhou, D. Li, L. Yang, C. Li, Y. Liu, J. Lu, Y. Wang, J. Mater. Sci. Mater. Electron. **28**, 7935 (2017)
46. O. Akhavan, Carbon **49**, 11 (2011)
47. A.A. Ashkarran, B. Mohammadi, Appl. Surf. Sci. **342**, 112 (2015)
48. S. Song, B. Cheng, N. Wu, A. Meng, S. Cao, J. Yu, Appl. Catal. B Environ. **181**, 71 (2016)
49. P. Wang, J. Wang, X. Wang, H. Yu, J. Yu, M. Lei, Y. Wang, Appl. Catal. B Environ. **132–133**, 452 (2013)

**Publisher's Note** Springer Nature remains neutral with regard to jurisdictional claims in published maps and institutional affiliations.